OCCAM, Oxford University

OCCAM Graduate Modelling Camp 2012 Report

Modelling of abrasive waterjet etching

Authors:
Charles Brett
Artur Gower
James Herterich
Klemens Katterbauer
Andrey Melnik
Julian Thompson

Supervisor:
Dr. John Billingham

May 27, 2014

1 Introduction

Waterjet etching is the process of using a waterjet for etching or engraving shapes and trenches from a material. The system is shown in Figure 1 where a high-pressure water inlet is attached to a jewel confining the water stream and increasing the speed. Garnet is introduced in order to improve the abrasive effect of the liquid whose composition gets close to be homogeneous via a mixing tube. A guard surrounds the mixing tube and the final waterjet liquid is impinging on the material.

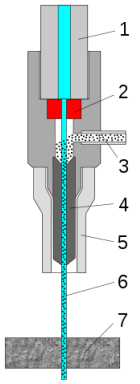

Figure 1: A diagram of a water jet cutter. (1): high-pressure water inlet. (2): jewel (ruby or diamond). (3): abrasive (garnet). (4): mixing tube. (5): guard. (6): cutting water jet. (7): cut material (source: waterjets.org)

The area of waterjet etching is mathematically relatively unexplored. Abdel - Rahman [1] presented a closed-form expression for an abrasive waterjet cutting model for ceramic materials while Kolahan et. al. [2] estimated and optimized the parameters of a linear model using a regression analysis. Lei et. al., [3] employed artificial neural networks for modeling abrasive water jet cutting for stainless steel while Yang et. al., [4] resorted to estimate parameters for optimizing the quality of an abrasive waterjet cutter. Popan et. al., [5] presented a study of the WJC etching process of steel and stainless steel material, however the mathematical models are mainly based on the estimation of a larger number of parameters that leaves a large number of degrees of freedom. Friedrich et. al., [6] resorted to the Kuramoto-Sivashinsky equation for modeling the ripple formation of the waterjet process. The work that was done by the mentor John Billingham is provided in the papers [7] and [8].

The major shortcomings of the models presented above is that they are

mainly based on statistical models that do not take into account the physical structure of the problem (ANOVA statistical model in Kolahan et. al., Neural Network modeling in Yang et. al.) or that they model waterjet cutting but not the etching process which requires a stronger coupling between the velocity and etching rate (WJC cutting model for ceramic materials by Abdel-Rahman, Artificial Neural Network model for WJC of steel by Lei et. al.). A further shortcoming is that even if the model physically represents the underlying structure, the obtained equation is complicated and difficult to solver numerically due to the inherent instabilities as in Friedrich et. al., where the Kuramoto-Sivashinsky equation given by

$$y_t = V(x)(f(y) + \alpha \triangle y + \beta \triangle^2) - u y_x \tag{1}$$

is used to model the problem. For a more detailed discussion and analysis of the Kuramoto-Sivashinsky equation, the reader may refer to the following publications by Hyman et. al. [9], and Boghosian et. al. [10].

2 Mathematical Modelling

2.1 Continuum approach

We assume that most of the etching is done by the impact of the garnet with the material, i.e. a high pressure jet of just water would not cut stone. Because of the large number of pieces of garnet which impact on the surface per second millimetre squared, we wish to formulate this as a continuum problem. We will argue this based on the typical dimensions of the jet we wish to model and the accuracy we wish to obtain. Note that the jet has a circular nozzel and let

R =jet diameter,

S = top speed that the jet machinery can move "parallel" to the surface.

$0.2R$ =garnet diameter,

VS = average velocity of the water leaving the jet,

where V is a large non-dimensional quantity. Assuming that on average the garnet particles leave the jet in a straight line, then for every point $\mathbf{X}$ on the surface we are etching (removing material), let θ be the angle between the trajectory of the garnet particle that hits $\mathbf{X}$ with the normal of the surface at the point $\mathbf{X}$, see Figure (2). We will, for the time being, consider that the average angle of impact is around $45°$, whilst noting that for extreme angles

the following my not hold true. Then the average surface area covered by the jet per unit time is $A_s = 2RS/\cos\theta = 2\sqrt{2}RS$. Now we'll approximate the number of garnet particles that leave the jet per unit time, G_s, as the volume of water that leaves the jet per unit time multiplied by the percentage of material assumed to be made of garnet, 20%, divided by the volume of a garnet stone.

$$G_s = \frac{0.2VS(R)^2\pi}{4(0.2R)^3\pi/3} \approx \frac{19VS}{R},$$

thus the average number of garnet stones that hit the surface, averaged over time, per area is given by

$$G_s/A_s \approx 7\frac{V}{R^2}.$$

The best precision we could hope for is about a tenth of the jets area, thus measuring area in this units we get that $R^2\pi = 4$, or

$$G_s/A_s \approx \frac{7}{10}\pi V,$$

where typically V is greater than 6000, thus a model that describes the influence of each individual stone, in a statistical or deterministic manner, is beyond our level of control and hence we prefer a continuum model.

2.2 The Model

We shall start with a simple example of the general model as to better our understanding. Suppose that the rate at which the height of a point $z(x, y)$ on the surface is etched is constant if the point is under the jet and zero if it is not under the jet, then assuming the jet is pointing along the z-axis In the simplest case the model is described by the equations:

$$\begin{aligned} \frac{\partial z}{\partial t} &= -H(\|\mathbf{X} - \bar{\mathbf{X}}(t)\|/R)P, \qquad t \in [0, T], \\ z(\mathbf{X}, 0) &= g(\mathbf{X}), \end{aligned} \tag{2}$$

where P is a constant representing the jet's etching power, $H(y) = 1$ if $0 \le y \le 1$ and 0 otherwise. The simplest case to test is $\bar{\mathbf{X}}(t) = (vt, 0)$. To do so we introduce the notation $f(\mathbf{X}) = z(\mathbf{X}, 0) - z(\mathbf{X}, T)$, let $\mathbf{X} = (x, y)$ then assuming that $\bar{X}(t)$ starts much before (x, y) and passes completely over (x, y) we can integrate both sides of equation (2) in t and obtain:

$$f(x, y) = -P \int_{-\sqrt{R^2-y^2}/v+x/v}^{\sqrt{R^2-y^2}/v+x/v} dt = -\frac{2P}{v}\sqrt{R^2 - y^2}. \tag{3}$$

Hence the transverse profile of the trench $z(x, \cdot, T)$ describes an ellipse who's eccentricity is determined by $2P/v$. Becuase the jet etching rate is uniform in its area of effect, we have that

$$f(\mathbf{X}) = -P\tau(\mathbf{X}), \tag{4}$$

where $\tau(\mathbf{X})$ is the exposure time of the point $\mathbf{X}$ under the jet, which is illustrated by equation (3).

There are two major effects that we have not taken into account in the above model. First, that garnet particles travelling closer to the jets central axis may travel faster than garnet particles travelling closer to the border of the jets tube. Therefore instead of using a step function we may want to use $M(\|\mathbf{X} - \bar{\mathbf{X}}(t)\|)$ with $M > 0$, which would allow for this behaviour. Second, if a garnet particle's velocity is orthogonal to the surface it hits, it will transfer more energy and thus etch away more material than a particle who's velocity is at an angle θ to the surface's normal vector. See Figure (2) below.

The general model we will present is phenomenological and below are some of the major the underling assumptions, it may be helpful to refer to the equations of the general model (6) whilst reading these assumptions. Though we first need,

Definition 1 *For each point on the surface, parametrized by* $\mathbf{X}$*, and time* t*, we call the point's ray: the shortest line from the jet's nozzel to the point on the surface.*

In a sense a ray is the continuum aproach which captures the average effect that the garnet stones have on a point on the surface. Now we present the model's major assumptions:

- The impact of the jet on the specimen results in the removal of material, and consequently changing its shape, only on the region of impact.
- The ray's length does not alter the rate at which material is removed.
- The rate at which material is removed by the jet depends on the angle θ between the surface normal and the point's ray.

According to the preceding we state the general pde as,

$$\frac{\partial z}{\partial t} = - M(\|\mathbf{X} - \bar{\mathbf{X}}(t)\|)A(\|\nabla z\|), \tag{5}$$

$$z(\mathbf{X}, 0) = g(\mathbf{X}) \tag{6}$$

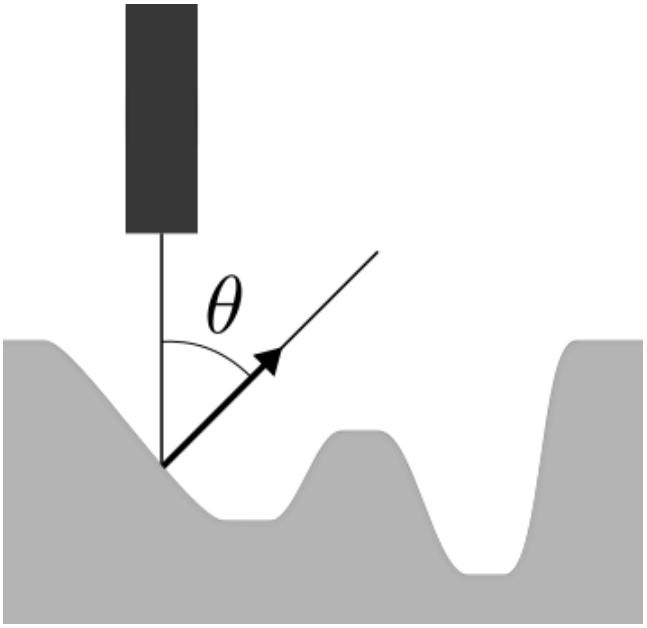

Figure 2: Example of one ray of the jet's ray's effect on the surface, where θ is the angle between the ray's direction and the surface normal.

where $\bar{\mathbf{X}}(t) \in \mathbb{R}^2$ is the parametrisation of the centre of the jet's effect on the surface, both $\bar{\mathbf{X}}(t)$ and $g(\mathbf{X})$ are given, M depends on the material and jet properties which hopefully will be determined by means of experimental data, and $A(\|\nabla z\|)$ capture's the dependence on θ noting that

$$\cos\theta = \frac{1}{(\|\nabla z\|^2 + 1)^{1/2}}.$$

Now to in fact determine M and A we must see in what form the experimental data is available. A most useful form of data would be to have the evolution of the surface in time while the jet stands still for several inclined planes. This could be done with some sort of laser inversion technology. Though for this project we were only presented with data for straight trenches, for which we would first have to solve the problem of inverting the trenches transversal profile to obtain M. To do so, assume the trench is sufficiently small so that we may take $A(\|\nabla z\|)$ to be approximately constant, or alternatively we could consider a function E that will capture in some respect the average $A(\|\nabla z\|)$ contribution to the decrease in z for approximately straight trenches, we shall come back to this argument after the

following: let $\bar{X}(t) = (vt, 0)$ then

$$\frac{\partial z}{\partial t} = E(\|(x - vt, y)\|), \tag{7}$$

for some undetermined function E, then

$$f(x,y) = \int_{-\sqrt{R^2-y^2}/v+x/v}^{\sqrt{R^2-y^2}/v+x/v} E(\|\mathbf{X} - (vt, 0)\|)dt = \int_{y}^{R} E(r)\frac{2r}{\sqrt{r^2 - y^2}}dt, \tag{8}$$

where we used the coordinate change for $r = \sqrt{(vt - x)^2 + y^2}$.

Note that along a straight trench the point X further away from the jet's axis, i.e. for a larger r in $E(r)$, would most likely be more inclined in relation to the jet's axis (z axis) and thus on average be etched away less then points where the jet's axis passed directly on top. Hence if $E(r)$ is not uniform, which experimental data will discern in posterior sections, this can either be explained by the function M in equation 6 being non-uniform, or by some average contribution of A.

3 Calibrating the general model

Recall that we started with a simple model which assumed uniform etching over the circular footprint of the jet. For straight jet paths this model predicted ellipse shaped trench cross-sections. However an ellipse is not observed in practice. This motivated us to consider the more general model (6):

$$\begin{aligned} \frac{\partial z}{\partial t} &= -M(||\mathbf{X} - \bar{\mathbf{X}}(t)||)A(||\nabla z||) \\ z(\mathbf{X}, 0) &= g(\mathbf{X}). \end{aligned}$$

This model says that the etching occurs at a rate that depends the distance from the centre of the jet (through the function M) and on the angle of the material being etched (through the function A). The goal of this section is to find forms of M and A which reproduce the experimental data.

To aid us in this task we solved (6) numerically using a simple first order forward Euler scheme. This allowed us to simulate the etching process, and hence investigate the affect of the form of M and A on the trench shape. We can see a snap shot of a simulation of the jet moving in a straight line in Figure 3.

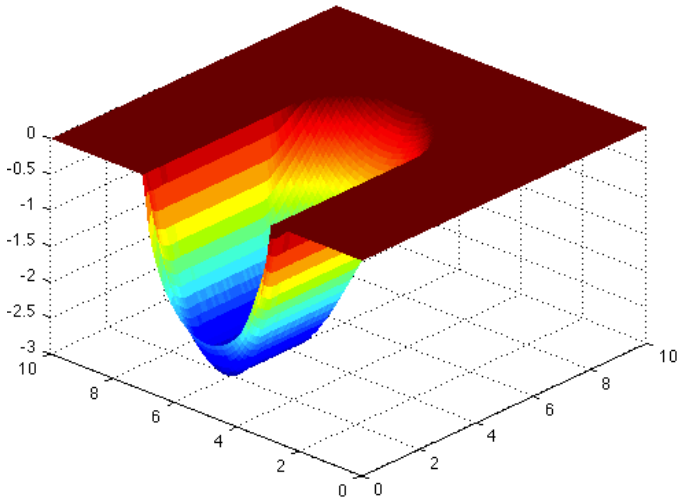

Figure 3: A simulation of the jet moving across the material.

3.1 Form of M

We initially ignore angle dependence by restricting our attention to shallow trenches. Therefore we just take A to be the identity. With this simplification we can actually derive an analytic expression for the radially symmetric etching function M in terms of the profile of the trench z produced when the jet moves in a straight line.

3.1.1 M in terms of z

We take a jet of circular aperture with radius R. The depth etched is determined by the amount of time a point is under the jet. For a jet moving at constant speed, this reduces to the width of the jet. Points closer to the centre line of the jet $y = 0$ spend more time under the jet and hence more etching occurs.

Let us consider a constant etching rate $M(r) = P$. The depth etched z is a function of the distance from the centre line of the jet. For a circular jet aperture, let us suppose that the jet moves at a constant speed v along the line $y = 0$. The width of the jet above a point $(\cdot, y)$ is the amount of exposure that point has to the jet. As such, it is easily deduced that

$$vz(y) = -2P\sqrt{R^2 - y^2}, \tag{9}$$

for $-R \leq y \leq R$. Hence, the depth etched out by a constant etching rate is elliptical.

Let us consider a more general etching rate $M(r)$. The depth $z(y)$ of the trench at a distance y from the centre line of the jet moving at constant speed v can be written as

$$vz(y) = 2\int_y^R \frac{M(s)\,s}{(s^2-y^2)^{\frac{1}{2}}}\,\mathrm{d}s, \tag{10}$$

for $0 \le y \le R$. The integral equation (10) can be solved in a similar way to the classical Abel Equation [11], with solution

$$\begin{aligned} M(r) &= \frac{1}{r}\frac{4}{\pi}\frac{\mathrm{d}}{\mathrm{d}r}\int_r^R \frac{vz(s)\,s}{(s^2-r^2)^{\frac{1}{2}}}\,\mathrm{d}s, &(11)\\ &= \frac{4v}{\pi}\frac{z(r)}{(R^2-r^2)^{\frac{1}{2}}} - \frac{4v}{\pi}\int_r^R \frac{z(s)-z(r)}{(s^2-r^2)^{\frac{1}{2}}}\,s\,\mathrm{d}s, &(12)\end{aligned}$$

for $0 \le r \le R$, where we assume that $M(R) = 0$. Hence, given data for $z(y)$ we can compute the etching rate $M(r)$.

3.1.2 M from experimental data

Now we can take the experimental data for shallow trenches and, after some preprocessing to make it symmetric, plug it into (12) to get M. The result of this can be seen in Figure 4.

Observe that the function in 4 approximately corresponds to a uniform etching in a central region and zero etching elsewhere. Therefore it is reasonable to take

$$M(||\mathbf{X} - \bar{\mathbf{X}}(t)||) := H(||\mathbf{X} - \bar{\mathbf{X}}(t)||/R), \tag{13}$$

where H is a heaviside function defined by

$$H(r) := \begin{cases} 1 & \text{if } r \le 1 \\ 0 & \text{if } r > 1 \end{cases},$$

and R is the radius of the active part of jet.

The simple form of (13) will make solving the inverse problem of section 4 easier. However, if we are just doing numerical simulations then we want M to be as accurate as possible, and the complexity of the function is not so much of a concern. Therefore instead of H we use a smooth approximation H_s to the heaviside function defined by

$$H_s(r) := \frac{1}{1+e^{2k(x-1)}}$$

for some parameter k. A value of $k = 15$ produces a function which closely matches the experimental data in Figure 4.

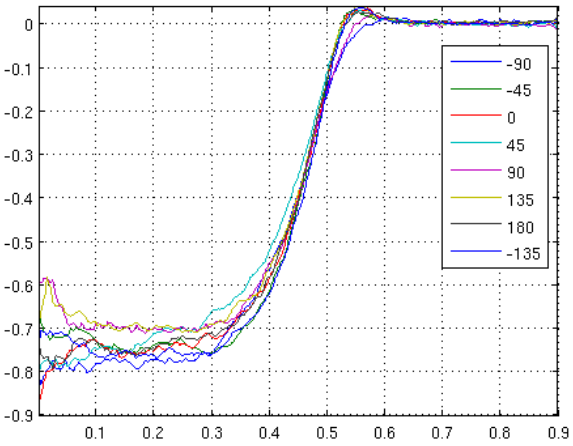

Figure 4: The function M corresponding to the experimental data for shallow trenches. Each line represents a cross-section at a different angle (in degrees) of a shallow pit made by the jet.

3.2 Form of A

Taking A to be the identity does not lead to a good approximation for deeper trenches. This is because of angle dependent effects, which we have confirmed from data showing that trenches are shallower when the jet hits the material at an angle. Unfortunately it is harder to find A in terms of z than it is to find M in terms of z. Therefore we resort to trying some physically reasonable forms of A and seeing how well the trenches the produced match the data we have.

In Figure 5 we can see some examples. The functions referred to in the legend are defined as follows:

- 'identity' - $A(||\nabla z||) := 1$
- 'normal velocity' - $A(||\nabla z||) := v_n$, were the normal velocity $v_n := \frac{v}{(||\nabla z||^2+1)^{1/2}}$
- 'cut-off' - $A(||\nabla z||) := \begin{cases} 1 & \text{if } v_n \geq C \\ 0 & \text{if } v_n < C, \end{cases}$ where C is a constant
- 'angle' - $A(||\nabla z||)$ is proportional to the angle of the material

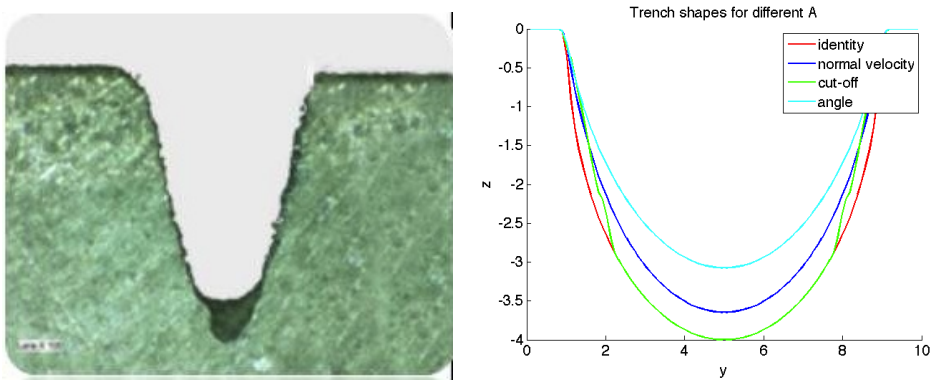

(a) Experimentally observed trench.

(b) Trenches generated by simulation.

Figure 5: Comparison of experimental data on deep trenches to simulated trenches for different forms of A.

We see that the 'cut-off' function produces a trench shape with fairly straight sides like in the experimental data. Therefore this may be a reasonable model for A. This is perhaps the best we can do with the limited amount of data we have available. In a collaboration with industry we could better determine A by running some experiments to get some data on the etching rate at lots of different angles, then interpolate this data to approximate A.

4 The Inverse Problem

Recently, industry has been most interested in how to etch a specific surface with these high pressured jets. This from our view point is an inverse problem, being that we have modelling the effect of the jet given a the jet's path and inclination. Solving such an inverse problem can be badly posed and overwhelming, so choosing which

parameters to take into consideration is crucial. In general, these might include: position of the jet's nozzle, angle of incidence, distance between the nozzle and the sample, jet properties such as its cross-section, properties of the material and many other. We have choosen to restrict ourselves to a simple and most influencial set of parameters, which are included in our model (6), to help achieve the inverse problem. Which can be formally

stated as

$$\frac{\partial z}{\partial t} = -M(\|\mathbf{X} - \bar{\mathbf{X}}(t)\|)A(\|\nabla z\|), \tag{14}$$
$$z(\mathbf{X}, 0) = g(\mathbf{X}) \quad \text{and} \quad z(\mathbf{X}, T) = f(\mathbf{X}) + g(\mathbf{X}),$$

where now $f(\mathbf{X})$ and $g(\mathbf{X})$ are given and the parametrization of the position of the centre of the jet's effect on the surface $\bar{\mathbf{X}}(t)$ is an unknown. We will consider both the 1D case as well as the full-dimensional case ($\bar{\mathbf{X}}(t) \in \mathbb{R}^2$). Anticipating things, we claim that in both cases there is neither an exact nor unique solution for an arbitrary $f(\mathbf{X})$.

4.1 Inverse problem in 1D

We shall first attempt to solve the 1D inverse problem for a uniform etching rate given by

$$\frac{\partial z}{\partial t} = -H((x - \bar{x}(t))/R),$$

where to simplify we take $z(x, 0) = 0$, thus

$$f(x) = -\int_{\|x - \bar{x}(t)\| \le R} dt = -\int_{x-R}^{x+R} \frac{d\bar{x}}{v(\bar{x})}, \tag{15}$$

this last step is achieved by means of a $\bar{x}(t)$ pushforward, in other words, $d\bar{x} = \partial_t \bar{x} dt = \bar{v} dt$, and the limits of integration are determined by $\|x - \bar{x}(t)\| = R$. Now differentiating both sides of the above equation in x gives us

$$f'(x) = \frac{1}{v(x - R)} - \frac{1}{v(x + R)}. \tag{16}$$

Note[1] that we wish to obtain v. Let us look first at the homogeneous part of the equation: $v_h(x - R) + v_h(x + R) = 0$, then if $v_h(x)$ is a solution then so is $v_h(x) + p(x, 2R)$ where $p(x, 2R) = p(x + 2R, 2R)$ for every x in the domain. This non-uniqueness of v can be rooted in the physics of the event by noting that if the jet speeds up and slows down periodically then the height of the surface will be etched on average as much as a jet moving at some intermediate speed, thus for these two cases the surface would be etched the same amount. To solve this we may enforce boundary conditions such as prescribing the limits $\lim_{x \to \pm\infty} v$.

[1] At this point the reader may wish to try out a simple example: $\bar{x}(t) = t^2/2$, $\partial_t \bar{x} = t$ thus $v(\bar{x}) = \sqrt{2\bar{x}}$ and substitute to see that the result make sense.

We may now work towards the inversion by substituting the Fourier transform of all functions in equation (16), then equating the integrands and renaming $\nu(\bar{x}) = 1/v(\bar{x})$, resulting in,

$$\hat{\nu}(k) = \frac{ik\hat{f}(k)}{e^{ikR} - e^{-ikR}}, \tag{17}$$

where

$$\hat{g}(k) = \frac{1}{\sqrt{2\pi}} \int_{-\infty}^{\infty} g(x)e^{-ikx}dx,$$

and we have thus assumed that for $x \to \pm\infty$ both $f(x)$ and $\nu(x)$ tend to zero, this also implies that the homogeneous solution to $\nu_h(k)(e^{-ikR} - e^{ikR}) = 0$ is possibly non-zero only on a zero-measure set, thus $\nu_h(x) = 0$. Now the singularities in $\hat{\nu}(k)$ occur at the points $kR = m\pi$ for $m \in \mathbb{N}$, these singularity in the frequency domain correspond to adding a $2R$-periodic function in the spatial domain, which is now not allowed by the boundary condition. To uphold the assumptions, when solving for $\nu(x)$ we must discard any $2R$-periodic function that might be added.

Now there is still the problem that once f is chosen and $\hat{f}$ found, then convergence of the inverse Fourier transform of $\hat{v}$ is by no means guaranteed, even for a very smooth function f. We present an example which convergence is certain, i.e. a spline defined on the interval $(x_0 - R, x_0 + R)$, so that

$$f(x) = H(R + x - x_0)H(R - x + x_0)\left(ax^3 + bx^2 + cx + d\right)$$

where,

$$H = \begin{cases} 1 & \text{if} \quad x \leq 0, \\ 0 & \text{if} \quad \text{otherwise.} \end{cases}$$

Using equation (17) this results in

$$\begin{aligned}\hat{\nu}(k) = &-\frac{e^{ikR-ik(R+x_0)}}{\sqrt{2\pi}}\left(x_0\left(3aR^2 + ax_0^2 + c\right) + b\left(R^2 + x_0^2\right) + d\right) \\ &+\frac{ie^{-ikx_0}}{\sqrt{2\pi}k^3}\left(3a\left(-2 + k\left(k\left(R^2 + x_0^2\right) - 2ix_0\right)\right) + k(2bkx_0 - 2ib + ck)\right) \\ &-\frac{iRe^{-ikx_0}}{\sqrt{2\pi}k^2}\cot(kR)\left(a\left(-6 + k\left(kR^2 + 3kx_0^2 - 6ix_0\right)\right) + k(2bkx_0 - 2ib + ck)\right).\end{aligned}$$

Now we remove the singularities in $\hat{\nu}$ that would lead to functions with a $2R$ period, then taking the inverse Fourier Transform we get

$$\begin{aligned}\nu(x) = &- \delta(x - x_0)\left(x_0\left(3aR^2 + ax_0^2 + c\right) + b\left(R^2 + x_0^2\right) + d\right) \\ &- \frac{1}{2}\mathrm{sgn}(x - x_0)\left(3a\left(R^2 + x^2\right) + 2bx + c\right) + 3aRx, \end{aligned} \tag{18}$$

the last term $3aRx$ was added so that equation (16) is satisfied, in other words we must have thrown something away inappropriately in $\hat{\nu}$. Now to illustrate this final result we plot both sides of equation (16) in Figure (6).

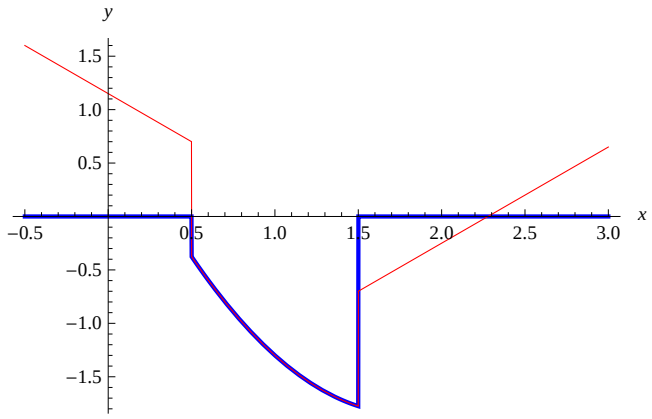

Figure 6: Where the blue line is $f'(x)$ and the red line is $\nu(x-R)-\nu(x+R)$.

This figure illustrates that the functions agree on the interval $(x_0 - R, x_0 + R)$, where $R = 0.5$ and $x_0 = 1$, it is also clear the difficulty of joining these splines together. For future considerations, after some experimentation with this analytic inverse, we have seen that $\hat{\nu}$ converges when an inversion is possible, as expected. One possibility is that when designing f we add a transition phase to the ends of the function f, just the same as where $\nu(x - R) - \nu(x + R)$differs from $f'(x)$. We could in fact use this previous solution to $\nu(x - R) - \nu(x + R)$ to add the appropriate transition phase. This phase brings about a multiplication of $\sin(kR)$ in $\hat{f}$ which could possibly guarantee the convergence of ν.

4.2 Inverse problem in 2D

The inverse problem in 2D does not have a solution in general, e.g. the non-existence of a solution is evident for $f(\mathbf{X})$, such that supp$f(\mathbf{X})$ is less than $2R$ in diameter. Since we deal with optimization, we use the notation $\tilde{f}(\mathbf{X})$

for the desired etching (i.e. from the inverse problem conditions) and $f(\mathbf{X})$ for the actual etching (i.e. current solution candidate provides). Here we provide some heuristic insights into the full-dimensional case of the inverse problem.

Equation (4) states that $f(\mathbf{X})$ and the exposure time $\tau(\mathbf{X})$ are proportional, hence we look for a way to control the exposure time. Our approach consists in choosing the path of jet motion, computing the jet motion speed which accounts for the exposure time at each point of the path Ξ, and obtaining the parametrization $\bar{\mathbf{X}}(t)$ from these. Assuming the nozzle speed v is constant throughout the whole route we have

$$f(\mathbf{X}) = -P\tau(\mathbf{X}) = \frac{P}{v} W(\mathbf{X}, \Xi), \tag{19}$$

i.e. the exposure time (and hence the amount of material) decomposes into the product of a path-independent term and the path function $W(\mathbf{X}, \Xi)$ (e.g. equation (3) means that $W(x, y, \Xi) = -2\sqrt{R^2 - y^2}$ for the straight line). One can choose v such that the desired etching $\tilde{f}(\mathbf{X})$ is achieved at a point $\mathbf{X}_0$ ($\tilde{f}(\mathbf{X}_0) = f(\mathbf{X}_0)$), or such that the actual etching matches the desired on average ($\int \tilde{f}(\mathbf{X}_0) d\mathbf{X} = \int f(\mathbf{X}_0) d\mathbf{X}$):

$$v_{exact} = \frac{PW(\mathbf{X}_0, \Xi)}{f(\mathbf{X}_0)}, \qquad v_{avg} = \frac{P \int W(\mathbf{X}, \Xi) d\mathbf{X}}{\int \tilde{f}(\mathbf{X}) d\mathbf{X}} \tag{20}$$

The relationship (19) can be extended for varying v: we split the entire domain into two regions corresponding to different constant values of v and parts of the path Ξ_1, Ξ_2 and a transitional region (naturally, a curve of width $2R$), which is to keep v continuous and separate the supports of $W(\mathbf{X}, \Xi_1)$, $W(\mathbf{X}, \Xi_2)$. For both sub-regions a suitable v_{avg} can be chosen and due to continuity considerations, $f(\mathbf{X})$ in transitional region is between the values of $\tilde{f}(\mathbf{X})$ in the sub-regions on average. Thus, disregarding $2R$-wide transitional regions the segmentation can be extended to the limit and still give an approximation

$$v(\mathbf{X}) \approx \frac{PW(\mathbf{X}, \Xi)}{f(\mathbf{X})} \approx \frac{PW(\mathbf{X}, \Xi)}{\tilde{f}(\mathbf{X})}. \tag{21}$$

To demonstrate this approach we first attempt to solve an inverse problem for $f(\mathbf{X}) = \text{const}$, that is, the task is to etch away a layer of material of constant depth. We use several equidistant parallel lines of length L as the path in order to scan the entire surface at the speed v, which is computed from (21).

a. b.

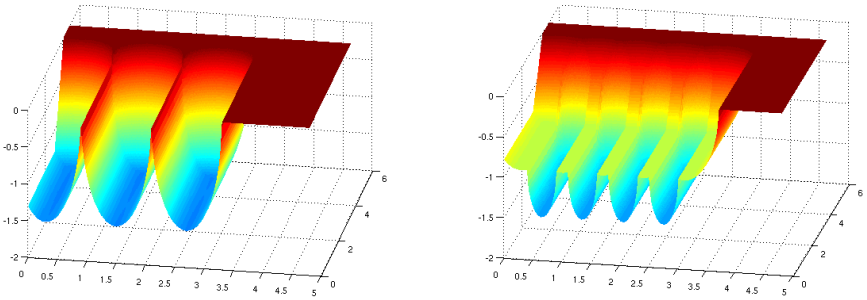

Figure 7: Numerical simulation of etching away a layer of material by several equidistant strokes: **a**. $n = 3$, stripes do not overlap; **b**. $n = 5$, stripes overlap.

Figure 7.a illustrates that the uniform etching together with circular jet cross-section results in an elliptic trench profile, and strokes with spacing $2R$, thereafter, result into equidistant furrows. The discrepancy between the desired and the actual surface measured in the uniform metric $\|f(x,y) - \tilde{f}(x,y)\|_\infty$ can be reduced by changing the nozzle route Ξ and, consequently, $W(\mathbf{X}, \Xi)$.

In particular, *'stripes overlapping'* strategy can be used: we increase the number of strokes n and decrease the distance between them, that improves the overall result as shown on Figure 7.b. In theory, the exact desired shape cannot be achieved using the 'stripes overlapping' strategy, since ellipses never add up to a rectangle. There is also a practical limitation of this strategy. Notice, that for uniform etching $\int f(\mathbf{X})d\mathbf{X} = -\frac{PL}{v}\pi R^2 n$ holds, therefore in order to keep this quantity constant one has to increase the number of stripes n in proportion to the nozzle velocity v, which is obviously bounded for technological reasons. Thus, the number of stripes is bounded as well.

In order to further illustrate the reverse problem in 2D, we are now looking for an approximate solution for axisymmetric shapes $f(\mathbf{X}) = f(r)$, where polar coordinates are introduced as follows: $\mathbf{X} = (x, y) = (r\cos\phi, r\sin\phi)$. We set the Archimedean spiral $\phi(r) = 2\pi r/\varepsilon$ as the path, where ε is the constant distance between successive turns measured along a radial ray. The speed $v(r)$ is varied to obtain the desired shape. Considering the spiral as the set of concentric circles and neglecting the curvature of the circles (that

makes a rather good approximation for large r) allows to write:

$$\begin{aligned} v(r) &\approx r\frac{d\phi}{dt} = \frac{2\pi r}{\varepsilon}\frac{dr}{dt}, \\ f(r) &\approx -\frac{P\pi R^2}{\varepsilon v(r)} \approx -\frac{PR^3}{2\varepsilon r\frac{dr}{dt}}, \end{aligned}$$

which leads to the ODE:

$$\frac{dr}{dt} = -\frac{PR^2}{2\varepsilon}\frac{1}{rf(r)}, \tag{22}$$

By solving the equation (22) with the initial condition $r(0) = 0$ (i.e. the spiral starts at the origin) one obtains the nozzle motion parametrization $\bar{\mathbf{X}}(t) = (\bar{x}(t), \bar{y}(t))$, which gives the approximate solution of the inverse problem:

$$\begin{aligned} r(t) &\quad -\text{the solution of (22)}, \\ \bar{x}(t) &= r(t)\cos\frac{2\pi r(t)}{\varepsilon}, \\ \bar{y}(t) &= r(t)\sin\frac{2\pi r(t)}{\varepsilon}. \end{aligned}$$

Notice, that if $f(x)$ is linear or piece-wise linear (i.e. defines a right circular cone or crown-like shape respectively), the equation (22) can be easily solved analytically by separation of variables.

The numerical simulation of etching axisymmetric shapes using this approach is depicted on Figure 8.

5 Conclusion

Waterjet technology has been a well-established and clean technology for performing high precision drills without facing the deteriorating effects of heat generation faced by other conventional drilling techniques. Despite its success in drilling, etching with waterjets has so far been hampered by the large number of degrees of freedom in the parameter calibration as well as that conventional models for waterjet cutting capture the etching process non-satisfactorily. In the report we have presented a general parameter dependent PDE model for simulating the waterjet etching process where the solution could be explicitly obtained in the 1 D case and in the 2 D case via an iterative inversion technique. Simulations show a perfect correspondence between the experimental data and the numerical results making accurate model predictions for waterjet etching a reality.

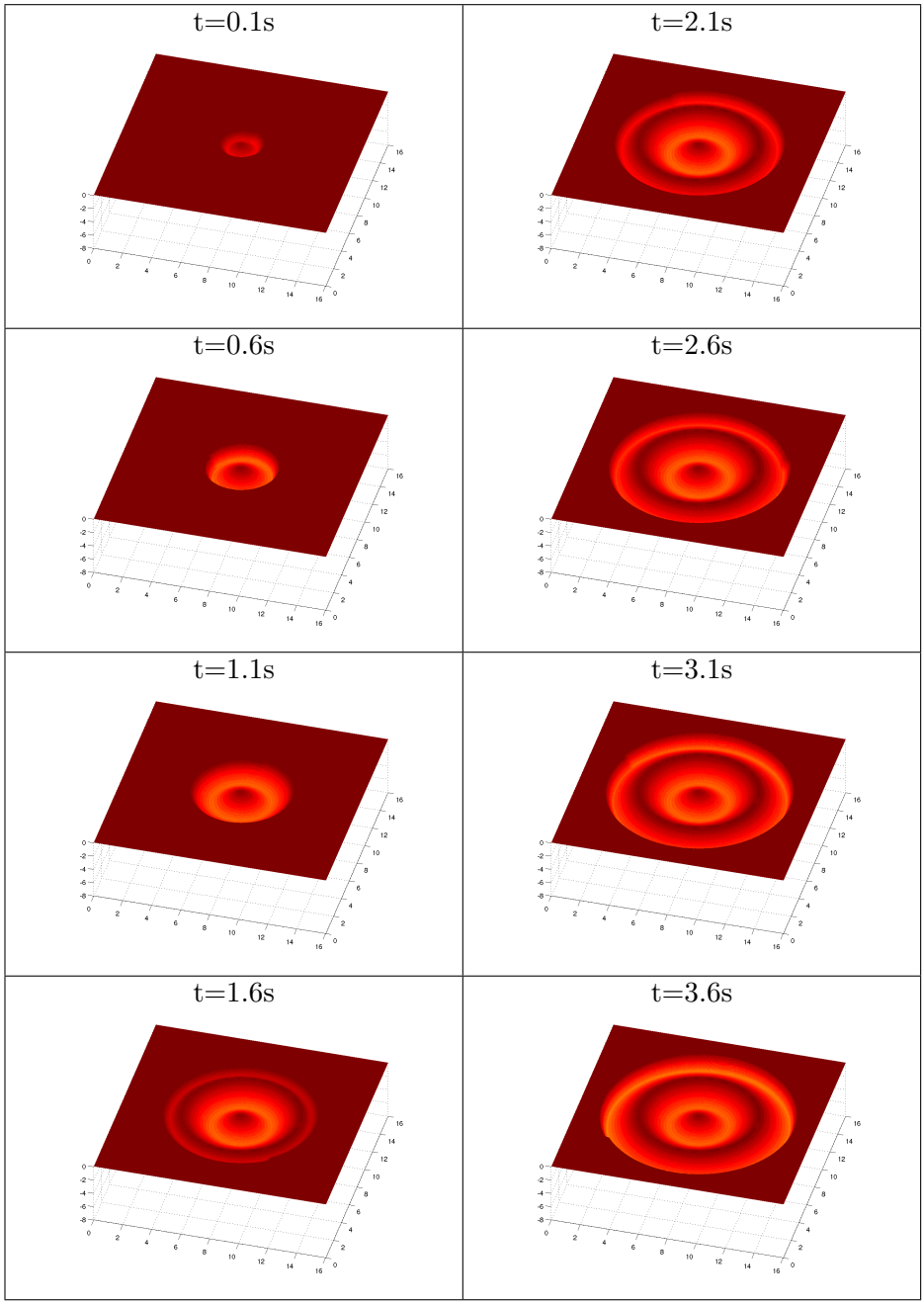

Figure 8: Etching of an axisymmetric shape. Length is measured in *mm*. .

References

[1] A. Abdel-Rahman, *A Closed-form Expression for an Abrasive Waterjet Cutting Model for Ceramic Materials*, Int. Journal of Mathematical Models and Method in Applied Sciences, 4, 5, 722-729 (2011)

[2] F. Kolahan et. al., *Modeling and Optimization of Abrasive Waterjet Parameters using Regression Analysis*, International Journal of Aerospace and Mechanical Engineering 5, 4 (2011)

[3] Y. Lei et. al., *Artificial Neural Network Model of Abrasive Water Jet Cutting Stainless Steel Process*, International Conference on Mechanic Automation and Control Engineering (MACE), 2010

[4] L. Yang et. al., *Neural network parametric modelling of abrasive waterjet cutting quality*, International Journal of Abrasive Technology, Vol. 1, No. 2, 198 - 207 (2007)

[5] I. A. Popan et. al., *A modeling study of the WJC etching process of steel and stainless steel materials.*, Annals of DAAAM & Proceedings, 2010

[6] R. Friedrich et. al., *Ripple Formation through an Interface Instability from Moving Growth and Erosion Sources.*,Physical Review Letters, Vol. 85 No. 23, (2000)

[7] J. Billingham et. al., *Geometrical modelling of abrasive waterjet footprints: a study for* 90° *jet impact angle* CIRP Annals - Manufacturing Technology, 2010, 59(1), 341-346.

[8] J. Billingham et. al., *Mathematical modelling of abrasive waterjet footprints for arbitrarily moving jets: Part Isingle straight paths*, Int. J. Mach. Tools & Manuf, 2012, 53, 58-68.

[9] J. M. Hyman et. al., *The Kuramoto-Sivashinsky equation: A bridge between PDE'S and dynamical systems*, Physica D, 18, 113-126 (1986)

[10] B. M. Boghosian et. al., *Hydrodynamics of the Kuramoto-Sivashinsky Equation in Two Dimensions*, Phys. Rev. Lett., 83, 5262-5265 (1999)

[11] D. Porter and D. S. G. Stirling, *Integral Equations*, Cambridge University Press (1990)